Journal of Solid State Chemistry 182 (2009) 3365–3373

Contents lists available at ScienceDirect

Journal of Solid State Chemistry

journal homepage: www.elsevier.com/locate/jssc

Yttrium-succinates coordination polymers: Hydrothermal synthesis, crystal structure and thermal decomposition

Zakariae Amghouz [a], Laura Roces [a], Santiago García-Granda [a], José R. García [a,*], Badredine Souhail [b], Luís Mafra [c], Fa-nian Shi [c], João Rocha [c]

[a] Departamentos de Química Física y Analítica y Química Orgánica e Inorgánica, Universidad de Oviedo, 33006 Oviedo, Spain
[b] Département de Chimie, Faculté des Sciences, Université Abdelmalek Essaâdi, 93002 Tétouan, Maroc
[c] Department of Chemistry, CICECO, University of Aveiro, 3810-193 Aveiro, Portugal

ARTICLE INFO

Article history:
Received 11 June 2009
Received in revised form
7 September 2009
Accepted 20 September 2009
Available online 9 October 2009

Keywords:
Yttrium
Succinate
Coordination polymer
Hydrothermal synthesis
Crystal structure
Thermal decomposition

ABSTRACT

New polymeric yttrium-succinates, $Y_2(C_4H_4O_4)_3(H_2O)_4 \cdot 6H_2O$ and $Y_2(C_4H_4O_4)_3(H_2O)_2$, have been synthesized, and their structures (solved by single crystal XRD) are compared with that of $Y_2(C_4H_4O_4)_3(H_2O)_2 \cdot H_2O$. Three compounds were obtained as single phases, and their thermal behaviour is described.

1. Introduction

The materials known as coordination polymers or MOF's, built from organic and inorganic units, represent one of the most active and attractive research fields in materials science, that has known a considerable development in the last decade, because of their structural diversity, and interesting properties, which lead to applications in areas such as gas (especially hydrogen) storage [1–9] and separation [10–13], catalysis [14–19], ion-exchange [20,21], magnetism [22,23], luminescence [24–27], or non-linear optics [28], and therefore open up the possibility of to creating novel multifunctional devices.

The flexible dicarboxylates ligands are much used in the synthesis of 2D and 3D coordination polymers, and present interesting properties, owing to both their diversity of coordination modes with metals, which may coexist in a given material, and to their conformational flexibility and ability to act as hydrogen-bond donors and acceptors. Among them, succinic acid adopts eclipsed, skew, opposed, and anti conformations, and possesses the ability to form frameworks with metal ions of different size [29,30]. The synthesis of such systems has been, mainly, focused on the use of transition metals. However, lanthanides (Ln) have received significant attention in the last years, because of their wide range of properties such as magnetism and photoluminescence. Ln^{3+} cations exhibit high affinity for oxygen [31], diverse coordination modes and variable coordination numbers [31,32]. Numerous works have been carried out using the hydrothermal synthesis route to prepare lanthanide coordination polymers of succinic acid [33–38], and some of them have investigated their luminescence [29,39,40], magnetic [30], and catalytic properties [41,42]. Nevertheless, to the best of our knowledge, there are only a few detailed studies reporting polymorphs of Ln(III)-succinic acid, either by using different synthetic methods, or by changing the reaction conditions [29,43].

Ruiz-Valero et al. [41] have reported the synthesis and structural characterization of the unique yttrium-succinate described up to now, $Y_2(C_4H_4O_4)_3(H_2O)_2 \cdot H_2O$. Its activity as heterogeneous catalyst makes the synthesis of other members in this family potentially interesting. These observations have prompted us to explore self-assembly in Y(III)-succinate systems. Here, we wish to report the hydrothermal synthesis and structural characterization of two novel yttrium-succinates coordination polymers, layered $Y_2(C_4H_4O_4)_3(H_2O)_4 \cdot 6H_2O$ and framework $Y_2(C_4H_4O_4)_3(H_2O)_2$. Two synthetic approaches were used: (i) changing the concentrations and succinate/yttrium ratios and

* Corresponding author.
E-mail address: jrgm@uniovi.es (J.R. García).

0022-4596/$ - see front matter © 2009 Elsevier Inc. All rights reserved.
doi:10.1016/j.jssc.2009.09.027

(ii) using additive ligands, such as terephthalic acid and trimellitic acid.

2. Experimental section

2.1. Synthesis

The yttrium-succinates, $Y_2(C_4H_4O_4)_3(H_2O)_2 \cdot H_2O$ (**1**), $Y_2(C_4H_4O_4)_3(H_2O)_4 \cdot 6H_2O$ (**2**) and $Y_2(C_4H_4O_4)_3(H_2O)_2$ (**3**) were synthesized under hydrothermal conditions.

For the preparation of **1**, 0.31 g (1 mmol) of $YCl_3 \cdot 6H_2O$, 0.17 g (1.5 mmol) of succinic acid was mixed in 15 mL of distilled water. After adjusting the pH value to 5 by addition of NaOH 1 M (*ca.* 1.5 mL) the reaction mixture was stirred at room temperature to homogeneity and then placed in a Teflon-lined stainless vessel (40 mL) and heated to 180 °C for 78 h under autogenous pressure and afterwards cooled to room temperature.

Compounds **2** and **3** were obtained in presence of terephthalic acid or trimellitic acid, respectively, with a synthesis procedure analogous to the preparation of **1**. Compound **2**: 0.31 g of $YCl_3 \cdot 6H_2O$ (1 mmol), 0.06 g of succinic acid (0.5 mmol), 0.08 g of terephthalic acid (benzene-1,4-dicarboxylic acid) (0.5 mmol) and 0.08 g of NaOH (2 mmol) in 10 mL of distilled water. Compound **3**: $YCl_3 \cdot 6H_2O$ (1 mmol), 0.06 g of succinic acid (0.5 mmol), 0.07 g of trimellitic acid (benzene-1,2,4-tricarboxylic acid) (0.33 mmol) and 0.08 g of NaOH (2 mmol) in 10 mL of distilled water.

In all cases, the resulting products were obtained as a single phase of colourless crystals. The solids were filtered off, washed thoroughly with distilled water, and finally air-dried at room temperature. The yield of such phase (based on Y) was of about 10% (**1** and **2**) or 15% (**3**).

We are still investigating this system, however, we have to admit that this system is very complicated to study. By using BDC and BTC, we have obtained pure phases with poor yield

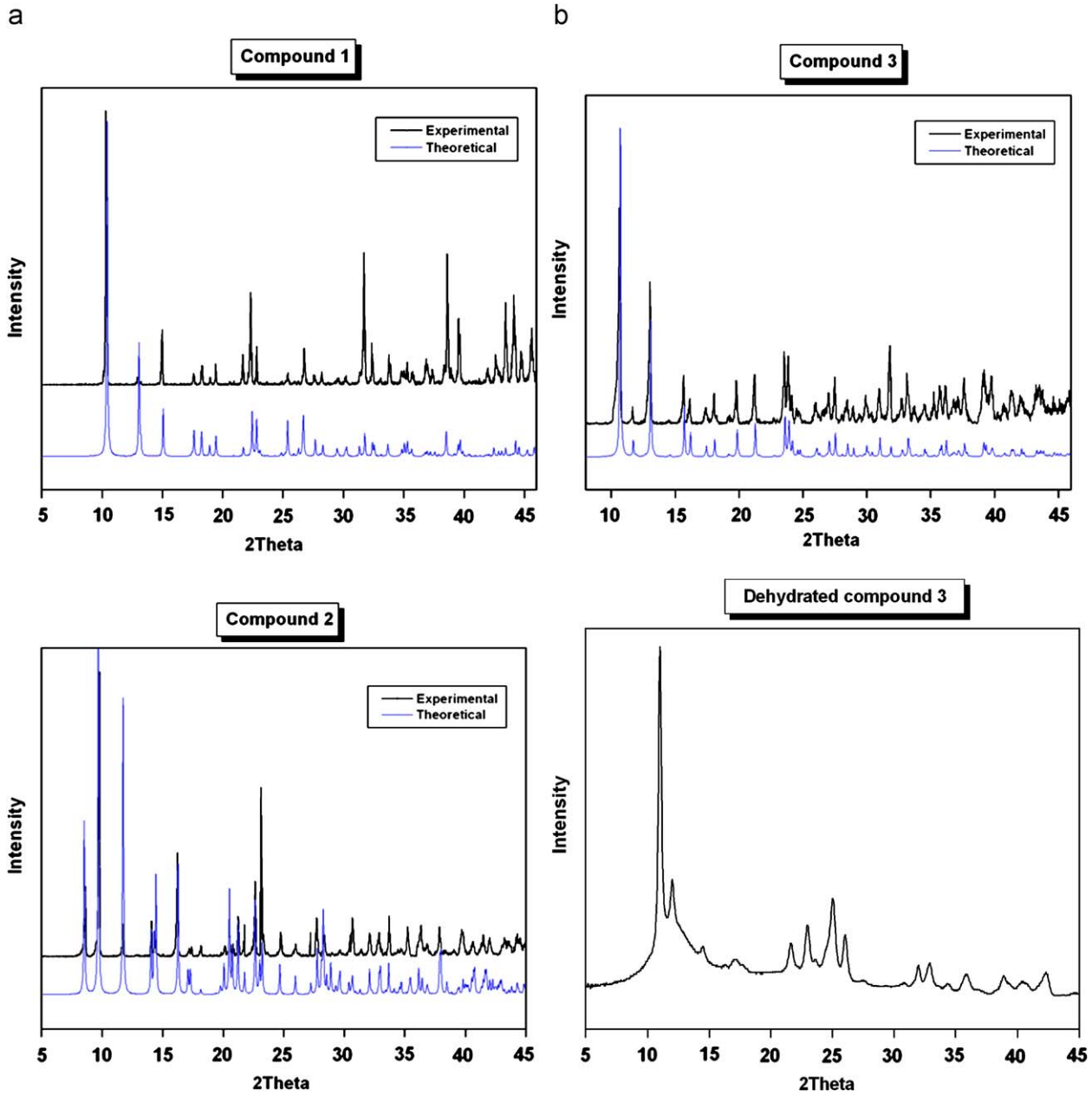

Fig. 1. XRD patterns of **1**, **2**, **3** compared with the theoretical ones (a) and dehydrated compound **3** (b).

(mentioned above), in most cases, by changing Y-succinic acid ratio/concentration, we obtain mixture of two phases belonging to the compounds **1** and **3**. The reaction yields are low, the optimisation of the synthesis conditions are needed. The use of the pH in the range of 5–6 is sufficient to deprotonate the carboxylate ligands used. At low pH value no phase has been formed. In the case of Y-BDC system, BDC crystalline was obtained, In the case of Y-BTC system no phase has been formed.

The X-ray powder diffraction patterns of the three compounds were preformed and compared with the theoretical ones (Fig. 1a). The powder XRD pattern of dehydrated **3** showed a poor crystallinity for this material (Fig. 1b). **1** shows a similar behaviour. For **2**, both dehydration and decomposition steps are overlapped.

2.2. Single-crystal X-ray diffraction studies

Data collection was performed at 293 K on a Oxford Diffraction Xcalibur Nova single crystal diffractometer, using Cu$K\alpha$ radiation (λ = 1.54180 Å). Images were collected at a 65 mm fixed crystal-detector distance, using the oscillation method, with 1° oscillation and variable exposure time per image. The crystal structure was solved by direct methods. The refinement was performed using full-matrix least squares on F2. All non-H atoms were anisotropically refined. All H atoms were either geometrically placed riding on their parent atoms or obtained from the difference Fourier map, with isotropic displacement parameters set to 1.2 times the Ueq of the atoms to which they are attached. Crystallographic calculations were carried out using the following

Table 2
Selected bond lengths (Å) and bond angles (°) for compounds **2** and **3**.

Compound 2			
Y(1)–O(8)	2.318(2)	C(1)–O(2)	1.252(4)
Y(1)–O(3)	2.330(2)	C(1)–O(1)	1.268(4)
Y(1)–O(7)	2.353(2)	O(2)–C(1)–O(1)	119.1(3)
Y(1)–O(1)	2.383(2)	C(4)–O(4)	1.246(4)
Y(1)–O(4)	2.394(2)	C(4)–O(3)^{I}	1.274(4)
Y(1)–O(5)	2.399(2)	O(4)–C(4)–O(3)^{I}	119.3(3)
Y(1)–O(6)	2.454(2)	C(5)–O(5)	1.267(4)
Y(1)–O(2)	2.489(2)	C(5)–O(6)	1.268(4)
Y(1)–O(3)^{I}	2.606(2)	O(5)–C(5)–O(6)	118.0(3)
Y(1)–Y(1)	4.113(2)		
Compound 3			
Y(1)–O(12)	2.3053(14)	C(1)–O(2)	1.240(3)
Y(1)–O(14)	2.3460(15)	C(1)–O(1)	1.277(2)
Y(1)–O(8)^{II}	2.3469(15)	O(2)–C(1)–O(1)	119.07(18)
Y(1)–O(6)^{II}	2.3704(14)	C(4)–O(3)	1.236(3)
Y(1)–O(1)	2.3945(14)	C(4)–O(4)^{IV}	1.285(3)
Y(1)–O(10)^{II}	2.4172(14)	O(3)–C(4)–O(4)^{IV}	119.63(19)
Y(1)–O(3)^{III}	2.4599(16)	C(5)–O(5)	1.248(3)
Y(1)–O(4)	2.4816(15)	C(5)–O(6)	1.281(2)
Y(1)–O(9)^{II}	2.5836(15)	O(5)–C(5)–O(6)	118.64(18)
Y(2)–O(7)	2.3075(14)	C(8)–O(7)	1.247(2)
Y(2)–O(9)	2.3189(15)	C(8)–O(8)	1.264(2)
Y(2)–O(1)	2.3917(14)	O(7)–C(8)–O(8)	124.89(18)
Y(2)–O(13)	2.3992(17)	C(9)–O(10)	1.256(3)
Y(2)–O(5)	2.4294(15)	C(9)–O(9)	1.267(2)
Y(2)–O(4)	2.4365(15)	O(10)–C(9)–O(9)	117.96(18)
Y(2)–O(11)	2.4623(15)	C(12)–O(12)	1.246(2)
Y(2)–O(2)	2.4802(16)	C(12)–O(11)	1.268(2)
Y(2)–O(6)	2.4810(14)	O(12)–C(12)–O(11)	124.96(18)
Y(1)–Y(2)^{II}	4.0001(2)		

Symmetry code: (I) $-x,-y+1,-z$; (II) $x-1, y, z$; (III) $x, y-1, z$; (IV) $x, y+1, z$.

Table 1
Crystallographic data for **2** and **3**.

Compound	**2**	**3**
Identification code	ZY2	ZY3
Empirical formula	C6 H16 O11 Y1	C12 H16 O14 Y2
Formula weight/g mol^{-1}	353.10	562.07
Temperature/K	293(2)	293(2)
Wavelength	Cu$K\alpha$ (1.54184 Å)	
Crystal system	Triclinic	Triclinic
Space group	*P*–1	*P*–1
Unit cell dimensions		
a (Å)	6.5328(2)	7.59090(10)
b (Å)	9.7828(4)	8.4348(2)
c (Å)	10.4889(3)	13.8238(3)
α (°)	80.2110(10)	97.104(2)
β (°)	89.831(2)	98.377(2)
γ (°)	71.378(2)	98.696(2)
Cell volume/Å^3	625.05(4)	855.94(3)
Z	2	2
Calc. Density/ mg m^{-3}	1.876	2.181
Absorption coefficient/ mm^{-1}	7.102	9.801
F(000)	358	556
Crystal size (mm^3)	0.204 × 0.093 × 0.016	0.197 × 0.0489 × 0.0108
Theta range for data collection/°	4.28–73.89	3.27–73.72
Index ranges	$-7 \le h \le 7, -12 \le k \le 12, -12 \le l \le 12$	$-9 \le h \le 9, -10 \le k \le 10, -17 \le l \le 17$
Reflections collected	8421	16920
Independent reflections	2385 [*R*(int)=0.0238]	3458 [*R*(int)=0.0245]
Completeness to theta=67°	97%	99.8%
Absorption correction	Refined (XABS2)	Refined (XABS2)
Max. and min. transmission	0.6094 and 0.3171	1 and 0.51424
Refinement method	Full-matrix least-squares on F^2	Full-matrix least-squares on F^2
Data/restraints/parameters	2385/9/193	3458/0/265
Goodness-of-fit on F^2	1.265	1.069
Final *R* indices [$I > 2$sigma(I)]	*R*1=0.0251, w*R*2=0.0714	*R*1=0.0215, w*R*2=0.0581
R indices (all data)	*R*1=0.0266, w*R*2=0.0855	*R*1=0.0221, w*R*2=0.0586
Largest diff. peak and hole	0.505 and −0.54 e Å^{-3}	0.584 and −0.333 e Å^{-3}

programs: CrysAlis CCD [44] for data collection; CrysAlis RED [45] for cell refinement, data reduction and empirical absorption correction; SHELX-97 [46] for structure solution; XABS2 [47] for refined absorption correction; SHELXL-97 for structure refinement and prepare materials for publication; PLATON [48] for the geometrical calculations; Diamond [49] for molecular graphics. Crystal data and structure refinement details for compounds **2** and **3** are outlined on Tables 1–3.

2.3. Thermal characterization

A Mettler-Toledo TGA/SDTA851^e and a DSC822^e were used for the thermal analyses in oxygen dynamic atmosphere (50 mL/min) at a heating rate of 10 °C/min. In all cases, *ca.* 10 mg of powder sample was thermally treated, and blank runs were performed. In TG tests, a Pfeiffer Vacuum ThermoStar^{TM} GSD301 T mass spectrometer was used to determine the evacuated vapours. The masses 18 (H_2O) and 44 (CO_2) were tested by using a detector C-SEM, operating at 1200 V, with a time constant of 1 s.

Table 3
Hydrogen-bond geometry in **1** [41], **2** and **3** (Å, °).

D–H···A	D–H [Å]	H···A [Å]	D···A [Å]	D–H···A [°]
Compound **1**				
O7–H7A···O1^{I}	0.76(7)	1.96(7)	2.717(5)	170
O7–H7B···O3^{II}	0.88(3)	2.02(4)	2.867(5)	161
Compound **2**				
O7–H7A···O1^{III}	0.72(5)	1.95(6)	2.675(3)	176
O7–H7B···O6^{IV}	0.74(6)	2.07(6)	2.799(4)	170
O8–H8A···O10^{IV}	0.87(7)	1.88(7)	2.728(5)	167
O8–H8B···O11	0.71(7)	1.99(6)	2.690(4)	169
O9–H9A···O10	0.94(3)	1.99(3)	2.928(5)	176
O9–H9B···O2^{V}	0.94(3)	2.12(4)	2.973(4)	150
O10–H10A···O2	0.95(4)	2.25(4)	3.073(4)	145
O10–H10A···O6	0.95(4)	2.33(4)	3.072(3)	135
O10–H10B···O11^{V}	0.95(4)	1.97(3)	2.851(4)	154
O11–H11A···O9	0.94(2)	1.85(2)	2.740(5)	159
O11–H11B···O5^{VI}	0.94(3)	1.81(3)	2.751(4)	178
Compound **3**				
O14–H14B···O10^{VII}	0.74(3)	2.00(3)	2.729(2)	174
O14–H14A···O11^{VIII}	0.78(3)	2.03(3)	2.791(2)	165
O13–H13A…O8	0.84(3)	2.05(3)	2.857(3)	162

Symmetry code: (I) 1/2−*x*, 1/2+*y*, 1/2−*z*; (II) 1/2−*x*, −1/2+*y*, 1/2−*z*; (III) −*x*, 1−*y*, −*z*; (IV) −1+*x*, *y*, *z*; (V) 1−*x*, −*y*, 1−*z*; (VI) −*x*, 1−*y*, 1−*z*; (VII) −*x*, 1−*y*, −*z*; (VIII) 1+*x*, −*y*, *z*.

3. Results and discussion

The structure of $Y_2(C_4H_4O_4)_3(H_2O)_2 \cdot H_2O$ (**1**) has already been found and described in the literature [41]. The asymmetric unit comprises one Y^{III} cation, one and half succinate anions, a coordinated water molecule and half uncoordinated water molecule. It is a three-dimensional framework, with empty channels running along the *c*-axis (Fig. 2a) with approximate dimensions of 7 × 3 Å, and with free water molecules located in the channels with approximate dimensions of 7 × 5 Å running along the *b*-axis (Fig. 2b). In the crystal structure, each Y^{III} cation coordinates to nine oxygen atoms (Fig. 3c) with tricapped trigonal prismatic coordination polyhedron joined in a chain edge-to-edge parallel to *b*-axis, the distance between adjacent Y in the chain is 4.0088(3) Å, these chains are in turn linked via succinate bridges in (001) and (101) directions, forming 3D framework. Eight of coordinated oxygen are carboxylic (O1–O2–O3–O4–O5–O6) and one from coordinated water molecule (O7). The three crystallographically independent carboxylate groups (coming from two different succinate anions one of them containing atoms O5 and O6 is situated on a crystallographic centre of inversion) may be divided into two groups according to their coordination mode: (i) the carboxylate group (O4–C4–O3) that acts as a bridge, coordinates each oxygen atom to a different Y^{III} cation; (ii) the two remaining carboxylates groups (O1–C1–O2) and (O6–C5–O5) coordinate one oxygen atom (O1, O6) to only one yttrium, and the other (O2, O5) acts as bridge between two different yttrium. In the structure, strong hydrogen bonds (see Table 3) between the aqua ligand (O7) and carboxylic oxygen atoms O1 and O3 contribute to strengthen the structure. We also suspect that the free water molecule (O8) participates in moderately strong hydrogen-bonding interactions with the aqua ligand (O7), in each case the aqua ligand acts as donor or acceptor, respectively.

Compound **2** is isostructural with several rare-earths succinates, $M_2(C_4H_4O_4)_3(H_2O)_4 \cdot 6H_2O$ (*M*=Ho, Er, Yb), previously reported [31,43,50]. The layered structure is built up from connections of Y^{III} cations and succinate ligands, with free water molecules located between the layers (Fig. 4). The asymmetric unit comprises one Y cation, one and half succinate anions, two coordinated water molecules and three uncoordinated water molecules. Each Y^{III} cation has nine-coordinated oxygen atoms (Fig. 3b), seven of them belonging to two succinate ligands and the two remaining belonging to two water molecules. The coordination polyhedra geometry can be described as a

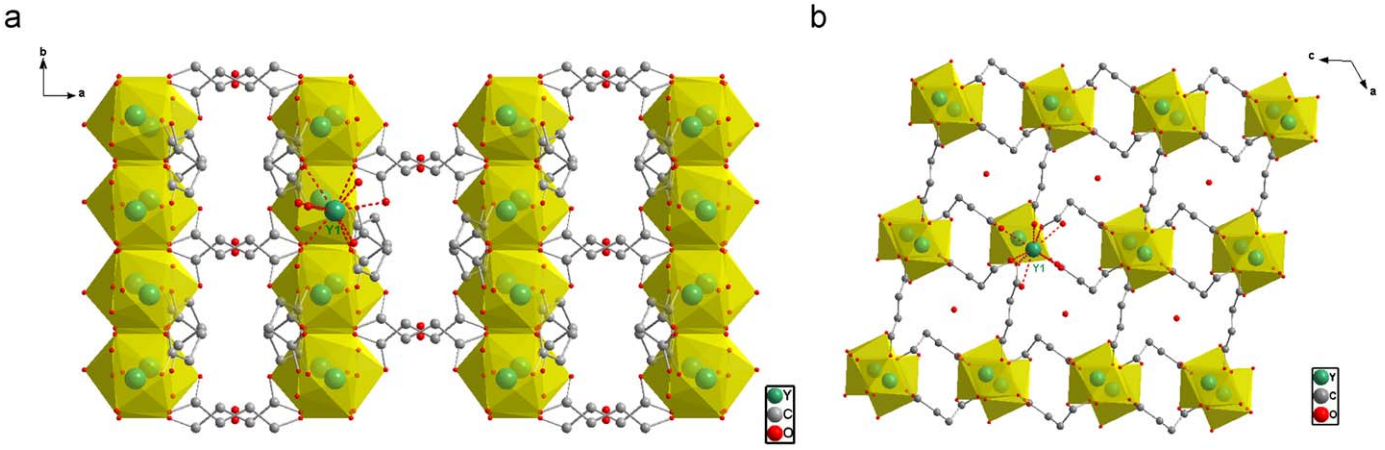

Fig. 2. Projection of the structure of **1** along the *c*-axis (a) and the *b*-axis (b).

monocapped square antiprism. Two edge sharing polyhedra, generate centrosymmetric dimmers Y_2O_{16} linked by succinate ions in (100) and (101) directions. The Y–O distances range from 2.318(2) to 2.606(2) Å and the average value is 2.414(2) Å. The distance between two adjacent Y cations within the bi-polyhedron is 4.114(2) Å. In this structure, there are two crystallographically independent succinate anions which have different coordination modes, one of which is situated on a crystallographic centre of inversion. This generates two carboxylate groups according two their coordination modes, the carboxylate groups (O2–C1–O1, O6–C5–O5) coordinate two oxygen atoms to only one yttrium (bond in chelating mode), and the remaining carboxylate group (O3–C4–O4) coordinates one oxygen atom (O4) to a single yttrium and the other (O3) bridges between two yttrium atoms. Moderate to strong interlayer hydrogen bonds are observed in **2** (see Table 3) providing 3D stability to the structure, involving uncoordinated water molecules (O8) which act as donor and uncoordinated water molecules (O10, O11) acting as acceptors, the latter (O10, O11) with (O9) act as donors with carboxylic oxygen atoms (O6, O5, and O2) of the succinate ligands, taking into account the contribution of hydrogen bonds between uncoordinated water molecules.

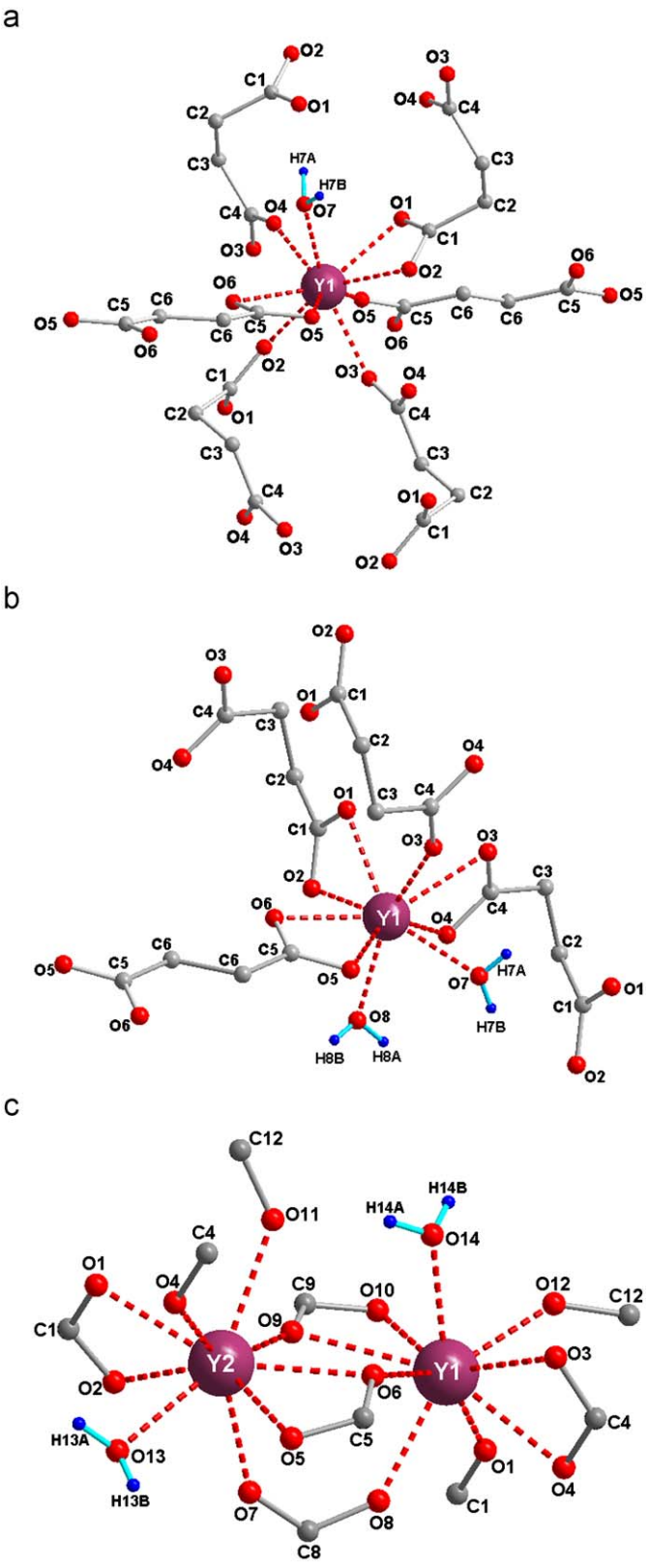

Fig. 3. Local coordination environment of the Y atom in **1** (a), **2** (b) and **3** (c).

Compound **3**, $Y_2(C_4H_4O_4)_3(H_2O)_2$, is isostructural with the corresponding erbium-analogue [51]. The asymmetric unit comprises two Y cations, three succinate anions, and two coordinated water molecules. The structure of **3** consists of a 3D framework (Fig. 5a) built from the connections of Y^{III} cation and succinate ligands. There are two crystallographically independent Y^{III}, both are nine-coordinated (Fig. 3a) within a tricapped trigonal prismatic geometry joined in a edge-to-edge chain parallel to the a-axis (Fig. 5b), defined by eight O atoms, derived from six carboxylate groups belonging to three different succinate anions and one molecular water, the chains are linked via succinate bridges in *b* and *c*-axis, forming the 3D framework. The Y1–O distances range from 2.3053(14) to 2.5836(15) Å and the average value is 2.4117(14) Å; similarly, related values for Y2–O are from 2.3075(14) to 2.4810(14) Å, and 2.4119(15) Å. The distance between adjacent Y1–Y2 cations in the chain is 4.0001(2) Å. The six independent carboxylate groups may be divided into two groups according to their coordination mode: the carboxylate groups (O8–C8–O7) and (O12–C12–O11) that act as a bridge, coordinate each oxygen atom to the two independent Y^{III}, the four remaining carboxylates groups coordinate one oxygen atom (O2, O3, O5, O10) to only one Y^{III}, while the other (O1, O4, O6, O9) bridges between two independent $Y1^{III}$ and $Y2^{III}$. In this structure, strong hydrogen bonds form (see Table 3) between the two coordinated water molecules (O13, O14) that act as donors, and carboxylic oxygen atoms of the bridging succinate ligands.

In the compounds **1** and **3**, the succinate ligands coordinated to yttrium adopt the same coordination modes, in contrast with compound **2** (see Scheme 1). Despite this, they present certain topological difference, which may be due to the different conformations of the succinate ligand. Although no free water molecules reside in the channels of **3**, in contrats with compound **1**, the structure is more compact and likely to be more stable than **1** and **2**. The presence of BTC in the reaction medium in the case of **3**, is manifested by more rich conformational modes (torsion angles) of succinate ligand, than **1** and **2**, and by maintained the same coordination modes of **1**. The presence of BDC in **2** is manifested by decreasing the carboxylate groups coordination number, and therefore high number of uncoordinated and coordinated waters molecules in **2**.

The thermal stability of **1**, **2** and **3** was investigated. The TG/DTG, SDTA curves, and the mass spectrometric analysis, are depicted in the Fig. 6, while Fig. 7 shows DSC traces. TG /DTG curves of **1**, **2** and **3** reveal total mass losses of, respectively, 60.6% (cal. 61.05%), 69.3% (cal. 68.01%), and 58.6% (cal. 59.78%), from room temperature up to 1000 °C, in good agreement with X-ray crystallography study, assuming Y_2O_3 is the final product of the decomposition (this has been confirmed by powder XRD).

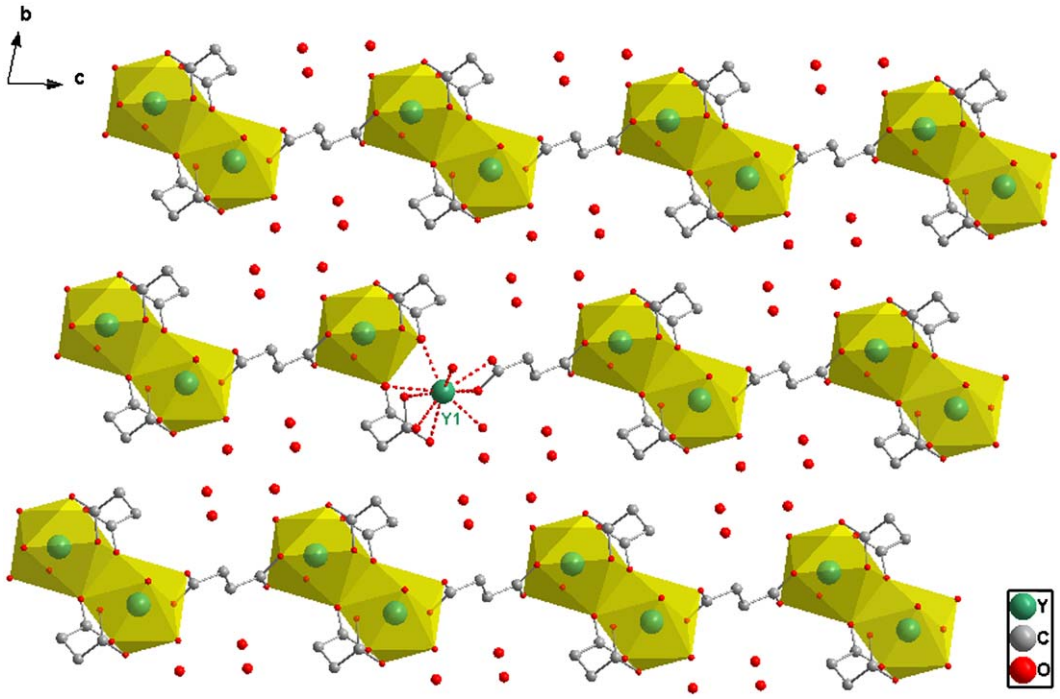

Fig. 4. Projection of the structure of **2** along the *a*-axis.

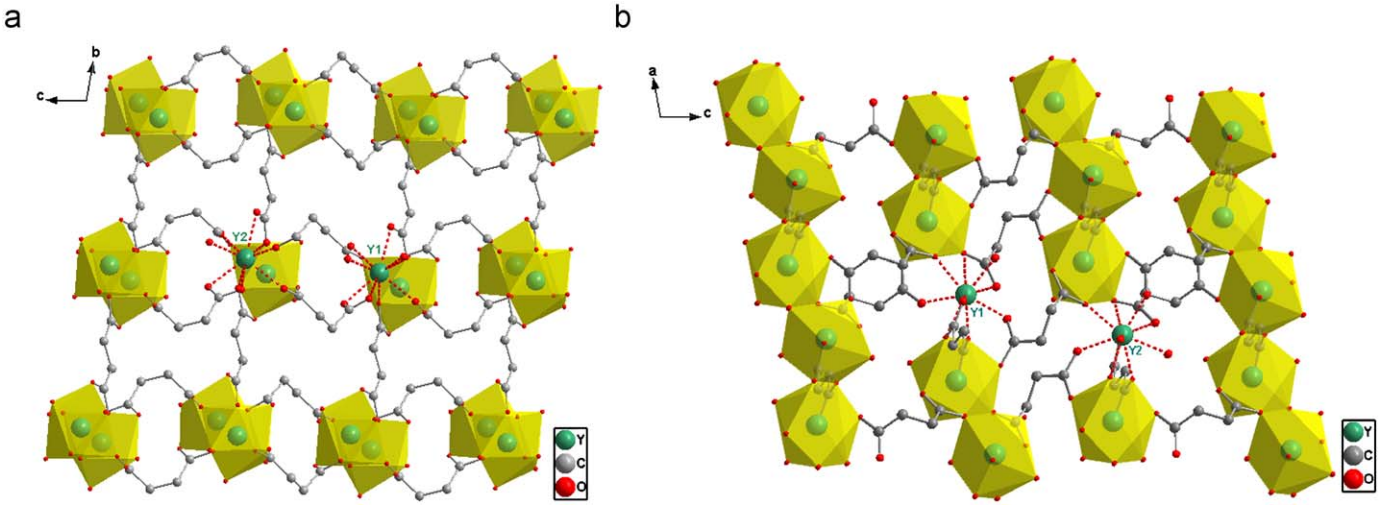

Fig. 5. Projection of the structure of **3** along the *a*-axis (a) and the *b*-axis (b).

The mass loss of **1**, in air, proceeds by two separate and defined steps. The first step between 120 and 200 °C (which reaches its maximum velocity at 180 °C), with the mass loss of 8.4% (cal. 9.31%), associated with endothermic peak at 190 and 200 °C on the SDTA and DSC curves, respectively, corresponds to the loss of *ca.* 3 (2.7 moles) water molecules: the free water molecule located in the channels and the two coordinated water molecules. The second step, between 330–900 °C, is complex, and composed of two continuous and overlapping processes with total mass loss of 52.1% (which reach their maximum velocity at 390 and 435 °C), and associated with exothermic peak which consists of two shoulders (at 385 and 410 °C) and a main peak on the SDTA (at 445 °C) and DSC (at 455 °C) curves, is assigned to the decomposition (oxidation) of the succinate ligand in two processes, which may be due to the partial collapse of channels after the water removal (dehydration step), leading to Y_2O_3. The

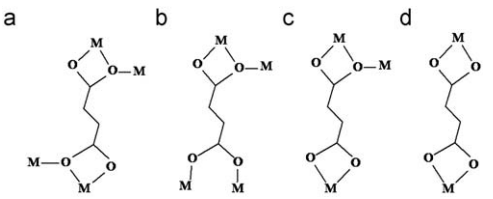

Scheme 1. (a) and (b): coordination modes of succinate ligands in compounds 1 and 3; (c) and (d): coordination modes of succinate ligands in compound 2.

associated mass spectrometry *m/z* 18 and 44 curves are in a good agreement with TG/DTG data. *m/z* 18 curve has two maxima, the first one at 190 °C corresponding to the loss of three water molecules, and the second at 445 °C (accompanied by a shoulder at 390 °C) coincides with the maximum of *m/z* 44 curve, which is

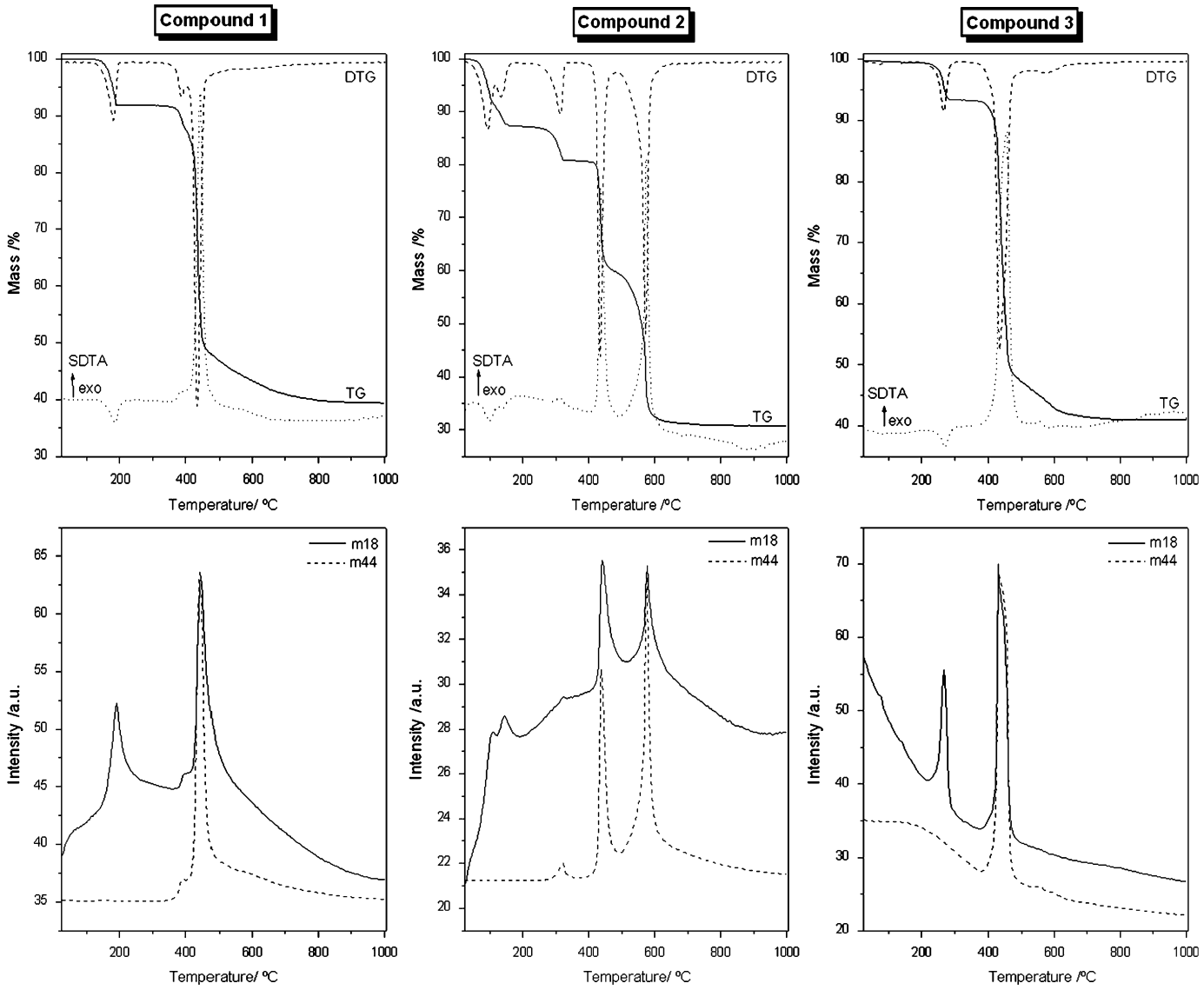

Fig. 6. TG-DTG-SDTA curves, and *m/z* 18 (H_2O) and *m/z* 44 (CO_2) MS signals of evacuated vapours, for **1**, **2** and **3**.

attributed to the decomposition step of the succinate ligand. Taking into account that the mass spectrometry analysis is a semiquantitative method, the integration of the first band (2868 nA) is almost half of the integration of the second one (5948 nA), proving the loss of six water molecules in the second step, corresponding exactly to the hydrogen atoms coming from the decomposition (or oxidation) of three succinic ligands in the formula of **1**. The rest of mass loss corresponding to the loss of CO_2, is showed by the maximum of *m/z* 44 curve at 450 °C.

The mass loss of **2** in air takes place in five stages. The first and the second stages are continuous, with the total mass loss of 12.8% (cal. 12.75%) in the range 50–200 °C (which reach their maximum velocity at 90 and 135 °C, respectively), associated with two endothermic peaks on the SDTA (at 100 and 140 °C) and DSC curves (at 110 and 145 °C), attributed to the loss of five uncoordinated water molecules located between the layers. The third stage between 200–350 °C, with the mass loss of 6.5% (reaches its maximum velocity at 315 °C), is simultaneously associated with endothermic and exothermic effects on the SDTA curve, and may be attributed to the loss of the last uncoordinated water molecule, and the beginning of the succinic acid oxidation. The DSC curve only exhibits an endothermic peak, which may be explained by a high endothermic effect making the exothermic peak unobservable. This multi-step dehydration behaviour of the uncoordinated water molecules can be explained as consequence of the hydrogen bonds existing between the uncoordinated water molecules, and their interactions with the coordinated water molecules. The fourth and the fifth stages are continuous, with mass losses of 20.9% and 28.9%, respectively, in the ranges 380–490 °C and 490–800 °C (reach their maximum velocity at 435 and 570 °C), associated with two exothermic peaks on the SDTA (at 435 and 570 °C) and DSC curve (at 440 and 580 °C), correspond to loss of the four coordinated water molecules and to the oxidation of the whole organic moiety leading to Y_2O_3 as residue. This three-step oxidation process may be due to the dimensionality of this compound (layered structures are known to undergo multistep decomposition processes). The associated mass spectrometry *m/z* 18 and 44 curves are in a good agreement with TG/DTG curves. The mass spectrometry *m/z* 18 curve has five maxima, the first and the second maxima at 110 and 145 °C, overlap and correspond to the loss of five interlayer water molecules; the third maximum at 450 °C coincides with the first

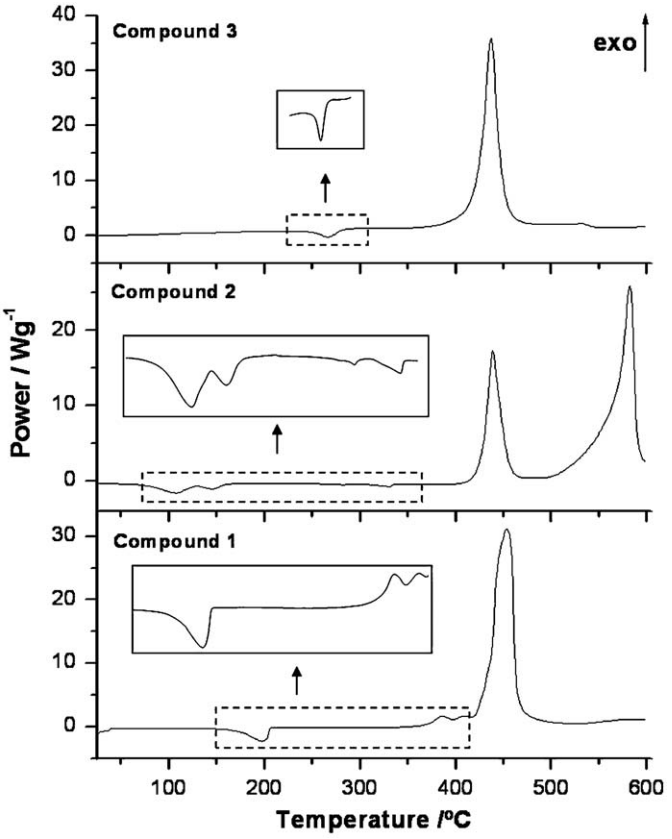

Fig. 7. DSC curves for **1**, **2** and **3**.

maximum of *m/z* 44 curve, which may be attributed to the loss of the last interlayer water molecule and to the first decomposition step of the succinic ligand. The fourth and the fifth maxima at 440 and 575 °C, coincide with the second and the third maxima of *m/z* 44 curve, and correspond to loss of the four coordinated water molecules and to the oxidation of the whole organic moiety leading to Y_2O_3 as residue. Taking in account that the mass spectrometry analysis is semiquantitative, the integration of the first three bands (4091 nA) is 0.78 of the integration of the fourth and fifth ones (5229 nA) in the *m/z* 18 curve, indicating the loss of approximatively ten water molecules in the fourth and fifth step, corresponding to four coordinated water molecules, and six water molecules resulting from the oxidation of the there succinic ligands in **2.** In the mass spectrometric *m/z* 44 curve, the integration of the three bands shows the loss of 0.30, 2.85 and 8.85 moles of CO_2 in the third, fourth and the fifth stages, respectively.

Similarly to **1**, the mass loss of **3** in air proceeds by two separate and defined stages. The first stage, with the mass loss of 5.9% (cal. 5.69%) in range 200–300 °C (which reaches its maximum velocity at 275 °C), described by endothermic effect on the SDTA (at 270 °C) and DSC curves (at 265 °C), is attributed to the loss of the two coordinated water molecules. The second stage is observed in the range 350–800 °C, with the corresponding mass loss of 52.7% (which reaches its maximum velocity at 440 °C), and described by exothermic peak on the SDTA and DSC curve at 450 and 435 °C, respectively, is attributed to one-step decomposition process of the whole organic moiety leading to Y_2O_3. The associated mass spectrometry *m/z* 18 and 44 curves are in a good agreement with TG/DTG data. *m/z* 18 curve has two maxima, the first one at 273 °C corresponding to the loss of the two coordinated water molecules, and the second one at 430 °C, which coincides with the maximum of *m/z* 44 curve. The integration of the first band (2577 nA) is almost a third of the integration of the second one (7235 nA), proving the loss of six water molecules in the second stage, corresponding exactly to the hydrogen atoms coming from the decomposition of three succinic anions in the formula, and the rest of mass loss corresponding to the loss of CO_2 showing by the maxima of *m/z* 44 curve at 430 °C.

The TG/DTG curves show that the compounds **1** and **3** have similar thermal decomposition behaviours. From the point of view of dehydration and the decomposition temperatures, the compound **3** is the most stable, followed by **1** and **2.** These results show that the 3D compounds are more stable than the layered ones. After the dehydration, the anhydrous compounds of **1** and **3** are stable up to 370 and 400 °C, respectively, and they have comparable oxidative decomposition enthalpies, 2888 and 2710 kJ/mol, respectively. Unlike **2,** the decomposition and the rest of dehydration steps (corresponding to loss of coordinated water molecules) occur simultaneously, which is reflected by an exothermic higher oxidative decomposition enthalpy (3601 kJ/mol), and this can be explained by the fact that the intermediate compound, partially dehydrated, is different from the anhydrous one in the case of **1** and **2**.

The structural reasons for such stability trend are the high number of uncoordinated and coordinated waters molecules in **2**; the uncoordinated water molecules residing in the channels of **1** which is manifested by large channels in **1** than in **3**; also the relatively shorter Y–O distances in **3** than in **1** and **2**, and finally the double infinite Y–O–Y connectivity along *b*-axis and *a*-axis in **1** and **3**, respectively, which is absent in the case of **2**, may explain the thermal stability order of the compounds.

4. Conclusions

The hydrothermal synthesis and crystal structure of new members in the yttrium-succinate family have been reported. The results suggest that the structural diversity obtained, in this system, is related to the coordination diversity and the conformational flexibility of the succinate ligand, which in turn depend on the synthesis conditions that play an important role in directing to one compound or another.

Supporting information available

CCDC nos. 735614 and 735615 contain the supplementary crystallographic data for compounds **2** and **3** described in this paper. These data can be obtained free of charge from The Cambridge Crystallographic Data Centre via http://www.ccdc.cam.ac.uk/data_request/cif.www.ccdc.cam.ac.uk/data_request/cif.

Acknowledgments

We thank financial support from FEDER, PTDC (Portugal), the Portuguese Foundation for Science and Technology (FCT), Spanish *Ministerio de Educación y Ciencia* (ACI20073448000507, MAT2006-01997 and *Factoría de Cristalización–Consolider Ingenio* 2010), and *Gobierno del Principado de Asturias* (PCTI 2006-2009).

Appendix A. Supplementary mateiral

Supplementary data associated with this article can be found in the online version at 10.1016/j.jssc.2009.09.027.

References

[1] S.S. Kaye, A. Dailly, O.M. Yaghi, J.R. Long, J. Am. Chem. Soc. 129 (2007) 14176.
[2] D.J. Collins, H.C. Zhou, J. Mater. Chem. 17 (2007) 3154.
[3] D. Sun, S. Ma, Y. Ke, D.J. Collins, H.C. Zhou, J. Am. Chem. Soc. 128 (2006) 3896.
[4] J.L.C. Rowsell, O.M. Yaghi, J. Am. Chem. Soc. 128 (2006) 1304.
[5] S. Ma, H.C. Zhou, J. Am. Chem. Soc. 128 (2006) 11734.
[6] A.G. Wong-Foy, A.J. Matzger, O.M. Yaghi, J. Am. Chem. Soc. 128 (2006) 3494.
[7] B.L. Chen, N.W. Ockwig, A.R. Millward, D.S. Contrereas, O.M. Yaghi, Angew. Chem. Int. Ed. 44 (2005) 4745.
[8] J.L.C. Rowsell, O.M. Yaghi, Micropor. Mesopor. Mater. 73 (2004) 3.
[9] G. Férey, M. Latroche, C. Serre, F. Millange, T. Loiseau, A. Percheron-Guegan, Chem. Commun. (2003) 2976.
[10] L. Pan, B. Parker, X. Huang, D.H. Olson, J.Y. Lee, J. Li, J. Am. Chem. Soc. 128 (2006) 4180.
[11] M. Dinca, J.R. Long, J. Am. Chem. Soc. 127 (2005) 9376.
[12] D.N. Dybtsev, H. Chun, S.H. Yoon, D. Kim, K. Kim, Am. Chem. Soc. 126 (2004) 32.
[13] R. Kitaura, K. Seki, G. Akiyama, S. Kitagawa, Angew. Chem. Intl. Ed. 42 (2003) 428.
[14] R.Q. Zou, H. Sakurai, Q. Xu, Angew. Chem. Int. Ed. 45 (2006) 2542.
[15] D.N. Dybtsev, A.L. Nuzhdin, H. Chun, K.P. Bryliakov, E.P. Talsi, V.P. Fedin, K. Kim, Angew. Chem. Int. Ed. 45 (2006) 915.
[16] W.B. Lin, J. Solid State Chem. 178 (2005) 2486.
[17] C.D. Wu, A. Hu, L. Zhang, W.B. Lin, J. Am. Chem. Soc. 127 (2005) 8940.
[18] L.G. Qiu, A.J. Xie, L.D. Zhang, Adv. Mater. 17 (2005) 689.
[19] B. Kesanli, W.B. Lin, Coord. Chem. Rev. 246 (2003) 305.
[20] O.M. Yaghi, H. Li, J. Am. Chem. Soc. 118 (1996) 295.
[21] A. Kamiyama, T. Noguchi, T. Kajiwara, T. Ito, Angew. Chem. Int. Ed. 39 (2000) 3130.
[22] Q. Ye, D.W. Fu, H. Tian, R.G. Xiong, P.W.H. Chan, S.P.D. Huang, Inorg. Chem. 47 (2008) 772.
[23] Q. Ye, Y.M. Song, G.X. Wang, K. Chen, D.W. Fu, P.W.H. Chan, J.S. Zhu, S.D. Huang, R.G. Xiong, J. Am. Chem. Soc. 128 (2006) 6554.
[24] W.J. Rieter, K.M.L. Taylor, W.B. Lin, J. Am. Chem. Soc. 129 (2007) 9852.
[25] B. Chen, Y. Yang, F. Zapata, G. Lin, G. Qian, E.B. Lobkovsky, Adv. Mater. 19 (2007) 1693.
[26] X.P. Yang, R.A. Jones, W.K. Wong, V. Lynch, M.M. Oye, A.L. Holmes, Chem. Commun. (2006) 1836.
[27] J.P. Zhang, Y.Y. Lin, X.C. Huang, X.M. Chen, J. Am. Chem. Soc. 127 (2005) 25495.
[28] O.R. Evans, W.B. Lin, Acc. Chem. Res. 35 (2002) 511.
[29] Y.F. Zhou, F.L. Jiang, D.Q. Yuan, B.L. Wu, M.Ch. Hong, J. Mol. Struct. 743 (2005) 21.
[30] S.C. Manna, E. Zangrando, A. Bencini, C. Benelli, N.R. Chaudhuri, Inorg. Chem. 45 (2006) 9114.
[31] N. Rahahlia, K. Alioune, A.G. Laidoudi, S. Dahaoui, C. Lecomte, Acta Crystallogr. Sect. E 62 (2006) 2543.
[32] H. Xu, J. Liang, J. Zhuang, H. Kou, R. Wang, Y. Li, J. Mol. Struct. 689 (2004) 177.
[33] F. Li, Acta Crystallogr. Sect. E 63 (2007) 840.
[34] Y.K. He, X.F. Wang, L.T. Zhang, Z.B. Hana, S.W. Ng, Acta Crystallogr. Sect. E 63 (2007) 3019.
[35] Q. He, J.F. Zi, F.J. Zhang, Acta Crystallogr. Sect. E 62 (2006) 1266.
[36] B. Yu, X.Q. Wang, R.J. Wang, G.Q. Shen, D.Z. Shen, Acta Crystallogr. Sect. E 62 (2006) 1620.
[37] C.X. Wang, Y. Li, Q.H. Zhang, D.J. Cai, X.B. Xie, Acta Crystallogr. Sect. E 62 (2006) 545.
[38] A. Seguatni, M. Fakhfakh, M.J. Vauley, N. Jouini, J. Solid State Chem. 177 (2004) 3402.
[39] B. Yu, C.Z. Xie, X.Q. Wang, R.J. Wang, G.Q. Shen, D.Z. Shen, J. Coord. Chem. (2007) 1817.
[40] G.H. Cui, J.R. Li, R.H. Zhang, X.H. Bu, J. Mol. Struct. 740 (2005) 187.
[41] J. Perles, M. Iglesias, C.R. Valero, N. Snejko, J. Mater. Chem. 14 (2004) 2683.
[42] J. Perles, M. Iglesias, C.R. Valero, N. Snejko, Chem. Commun. (2003) 346.
[43] M.C. Bernini, E.V. Brusau, G.E. Narda, G.A. Echeverria, C.G. Pozzi, G. Punte, C.W. Lehmann, Eur. J. Inorg. Chem. (2007) 684.
[44] CrysAlis CCD, Oxford Diffraction Ltd., Version 1.171.32.37 (release 24-10-2008 CrysAlis171 .NET) (compiled Oct 24 2008,09:44:38).
[45] CrysAlis RED, Oxford Diffraction Ltd., Version 1.171.32.37 (release 24-10-2008 CrysAlis171 .NET) (compiled Oct 24 2008,09:44:38).
[46] G.M. Sheldrick, SHELXL-97, Program for refinement of crystal structures, University of Göttingen, Germany, 1997.
[47] S. Parkin, B. Moezzi, H. Hope, J. Appl. Crystallogr. 28 (1995) 53.
[48] [a] A.L. Spek, Acta Crystallogr. Sect. A. 64 (1990) 34;
[b] A.L. Spek (Ed.), PLATON, A Multipurpose Crystallographic Tool, Utrecht University, Utrecht, The Netherlands, 1998.
[49] K. Brandenburg, DIAMOND. Version 3.1. 2007, Crystal Impact GbR, Bonn, Germany.
[50] J. Sun, Y.Q. Zheng, J.L. Lin, Z. Kristallogr, New Cryst. Struct. 219 (2004) 99.
[51] G.Y. Dong, G.H. Cuia, J. Linb, Acta Crystallogr. Sect. E 62 (2006) 738.